Supplemental Fig.1

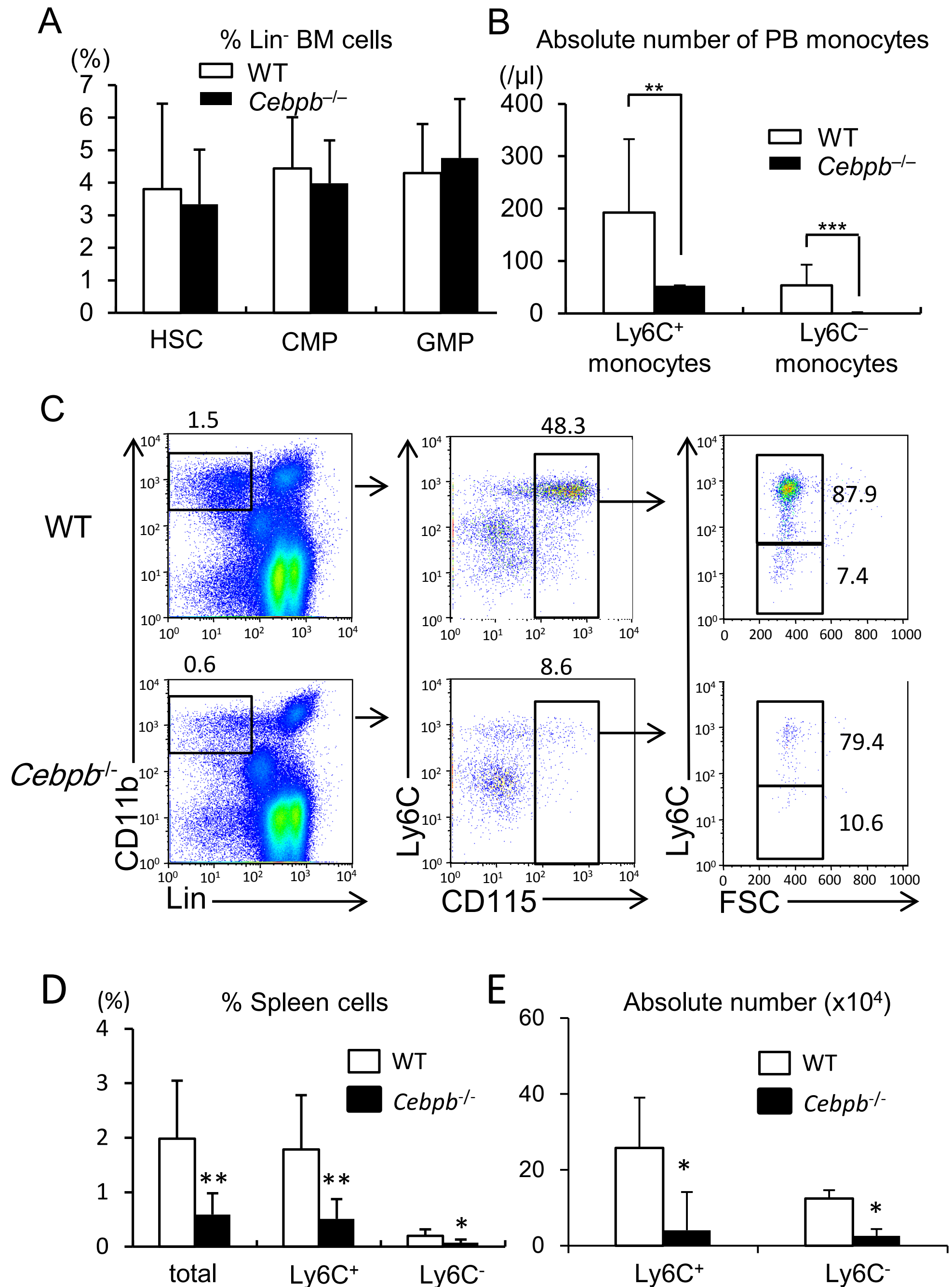

Figure S1

Specific decrease in monocytes in *Cebpb*$^{-/-}$ mice.

(A) Frequencies of HSCs, CMPs, and GMPs among lineage^{-} BM cells from WT or *Cebpb*$^{-/-}$ mice (n=5). (B) Absolute numbers (/µl) of Ly6C^{+} and Ly6C^{-} monocytes in PB of WT or *Cebpb*$^{-/-}$ mice (n=13). (C) Representative flow cytometric analysis of Ly6C^{+} and Ly6C^{-} monocytes in the spleen of WT or *Cebpb*$^{-/-}$ mice. (D) Frequencies of total, Ly6C^{+} and Ly6C^{-} monocytes in the spleen of WT (n=10) or *Cebpb*$^{-/-}$ (n=10) mice. (E) Absolute numbers of Ly6C^{+} and Ly6C^{-} monocytes in the spleen of WT (n=5) or *Cebpb*$^{-/-}$ (n=5) mice. Data are presented as mean ± SD. *p<0.05, **p<0.01, ***p<0.001.

Supplemental Fig.2

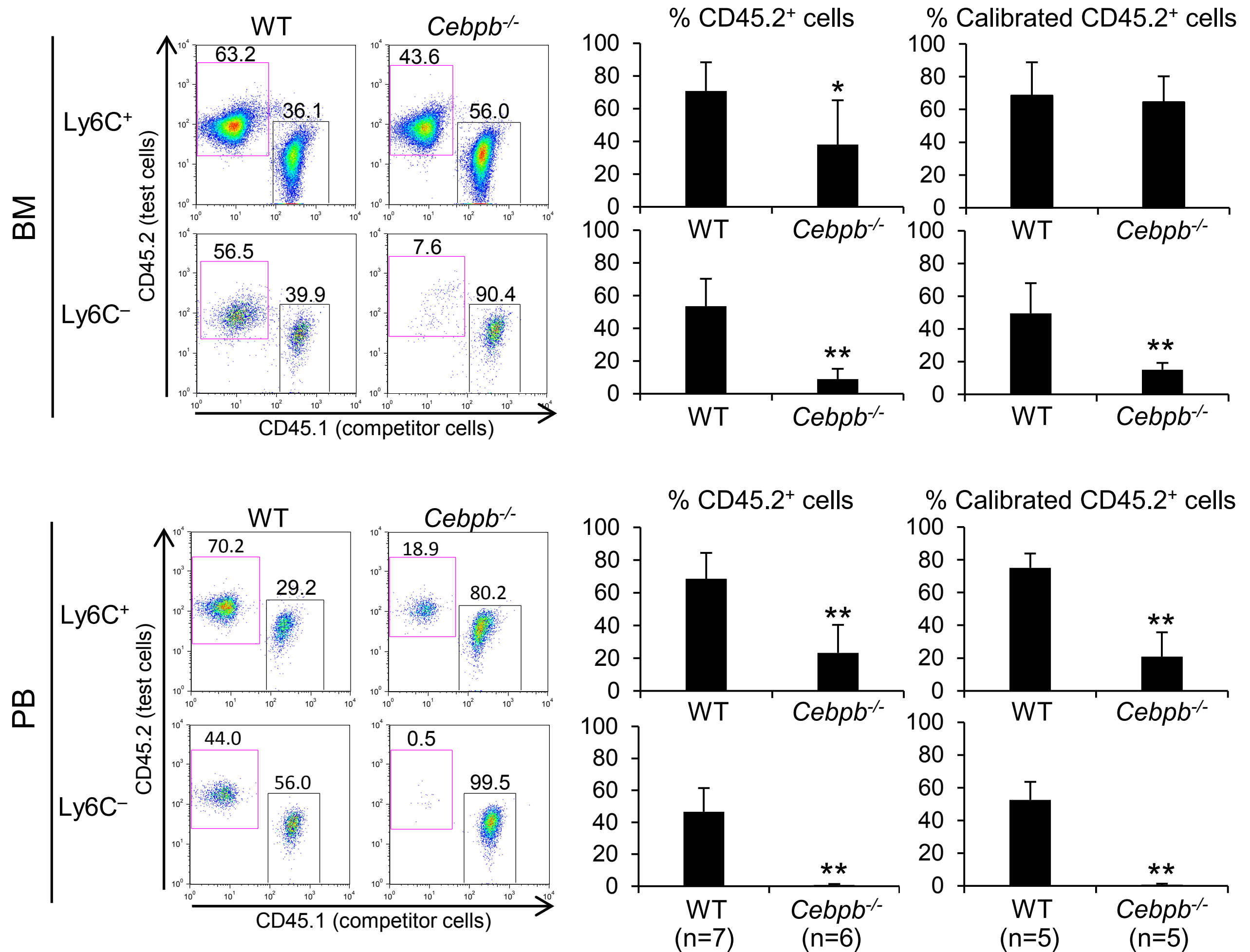

Figure S2

Competitive BM transplantation reveals the cell-intrinsic requirement of C/EBPβ for monopoiesis.

A total of 5×10^5 BM cells from WT or *Cebpb*$^{-/-}$ mice (CD45.2$^+$) together with 5×10^5 WT BM cells (CD45.1$^+$) were transplanted into lethally irradiated (8 Gy) WT recipient mice (CD45.1$^+$). Six weeks later, BM and PB samples were analyzed by flow cytometry. Expression of CD45.1 and CD45.2 on the indicated monocyte subsets is shown. Chimerism of *Cebpb*$^{-/-}$ cells was significantly lower at the HSC level (unpublished observation). Therefore, the frequencies of CD45.2$^+$ test cells in the indicated monocyte subsets (middle panel) were calibrated according to CD45.2$^+$ chimerism among c-kit$^+$ Sca-1$^+$ lineage$^-$ HSCs (right panel). Data are presented as mean ± SD. *$p<0.05$, **$p<0.01$.

Supplemental Fig.3

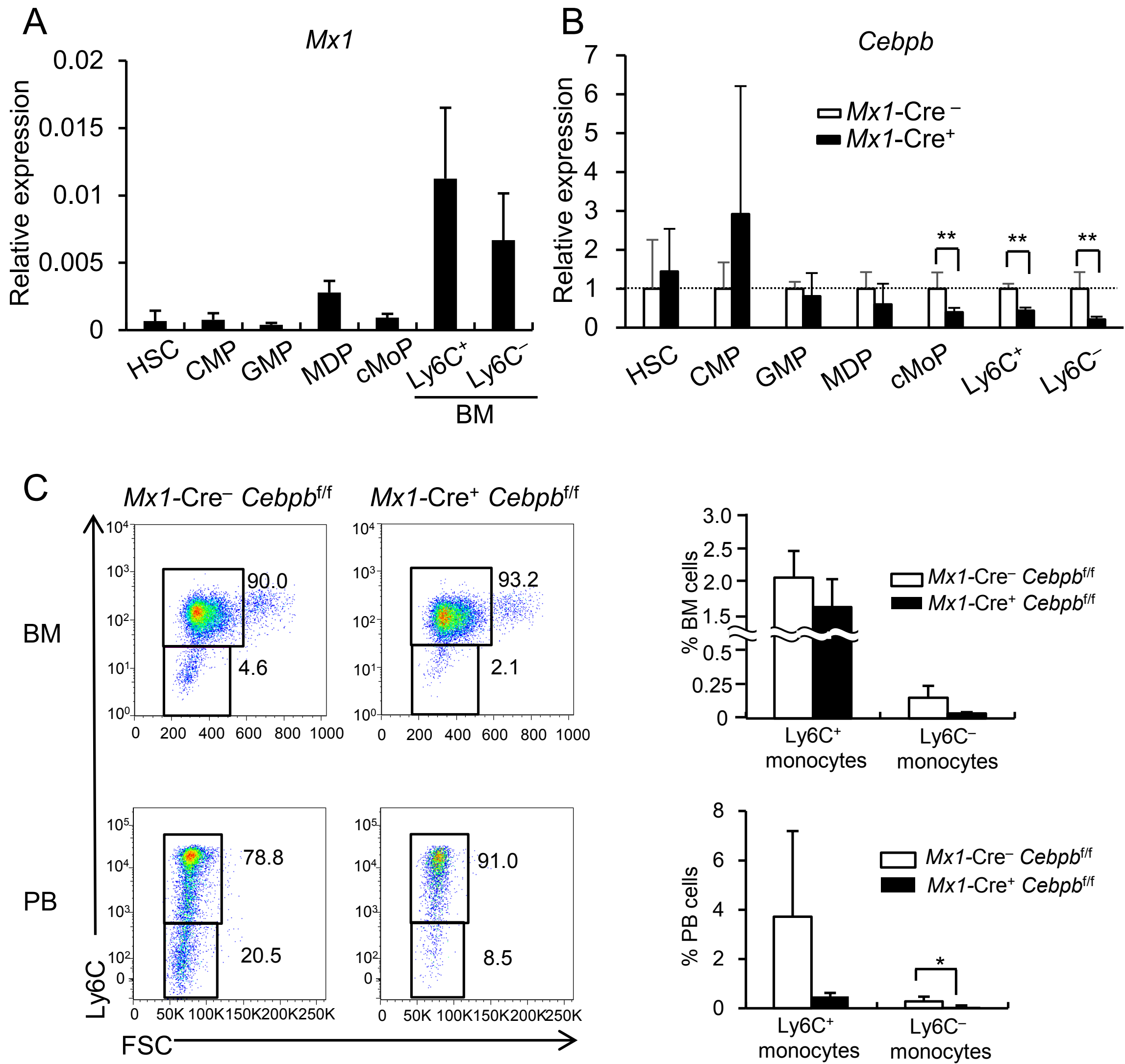

Figure S3

Specific targeting of monocytes in *Mx1*-Cre transgenic mice.

(A) *Mx1* mRNA was upregulated during differentiation into monocytes. Quantitative RT-PCR of *Mx1* expression in HSCs, CMPs, GMPs, MDPs, cMoPs, Ly6C$^+$ monocytes, and Ly6C$^-$ monocytes purified from BM of WT mice by cell sorting (n=3). (B) *Cebpb* mRNA expression in the indicated cell populations obtained from BM of *Cebpb*$^{f/f}$ mice or mice produced by crossing *Cebpb*$^{f/f}$ mice with *Mx1*-Cre transgenic mice (n=3). (C) Frequencies of Ly6C$^+$ and Ly6C$^-$ monocytes in BM and PB of *Cebpb*$^{f/f}$ mice (n=6) or mice produced by crossing *Cebpb*$^{f/f}$ mice with *Mx1*-Cre transgenic mice (n=7). Data are presented as mean ± SD. *p<0.05, **p<0.01.

Supplemental Fig.4

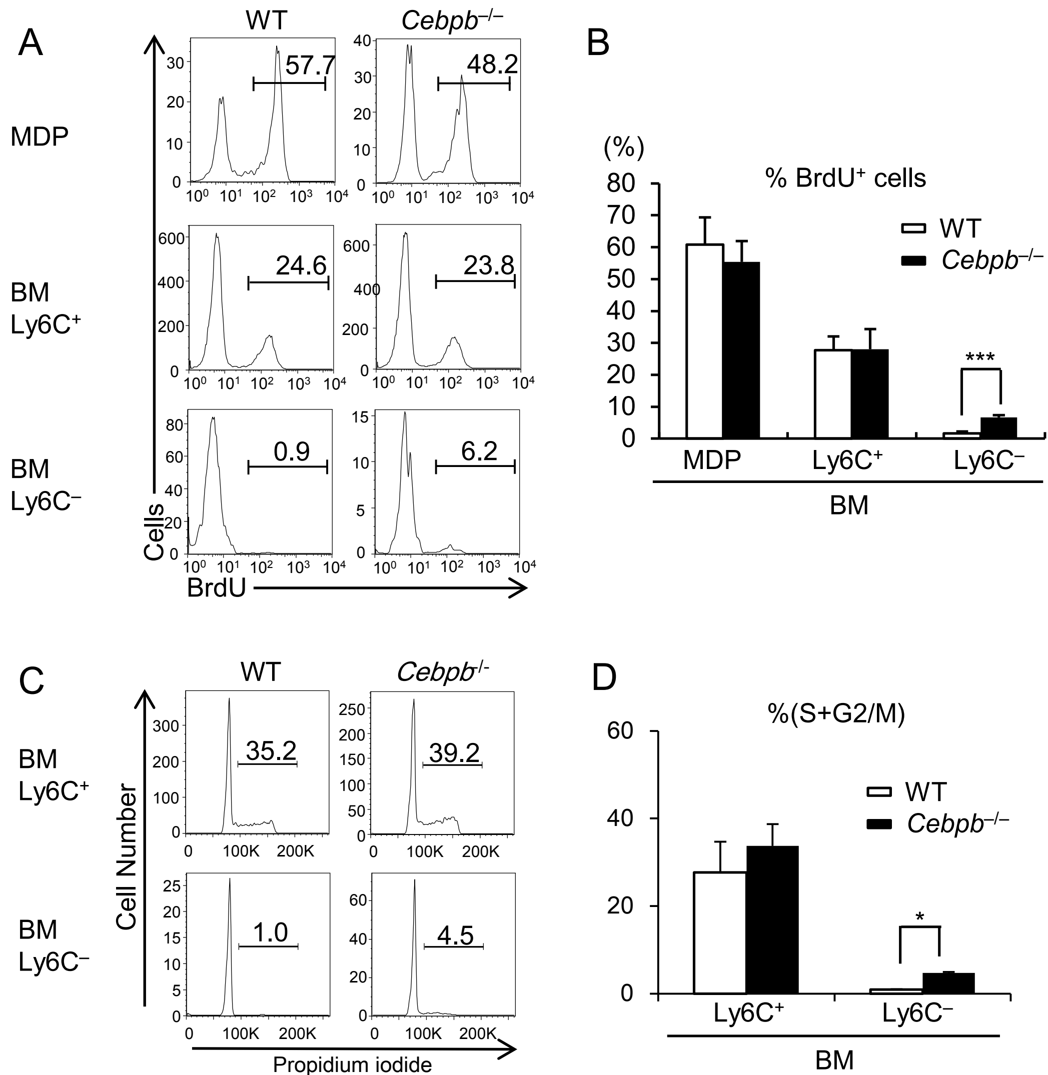

Figure S4

The cell cycle status of monocytes in the absence of C/EBPβ.

(A) Flow cytometric analysis of BrdU incorporation in MDPs, Ly6C+ monocytes, and Ly6C– monocytes obtained from BM of WT or *Cebpb*–/– mice. (B) Frequencies of BrdU+ cells in each population from WT or *Cebpb*–/– mice (n=3). (C and D) Ly6C+ or Ly6C– monocytes were purified from WT (n=3) and *Cebpb*-/- (n=3) mice, fixed with ethanol, and subjected to cell cycle analysis using propidium iodide staining. The proportions of cycling cells (in S/G2/M phases) are shown. Data are presented as mean ± SD. ***p<0.001.

Supplemental Fig.5

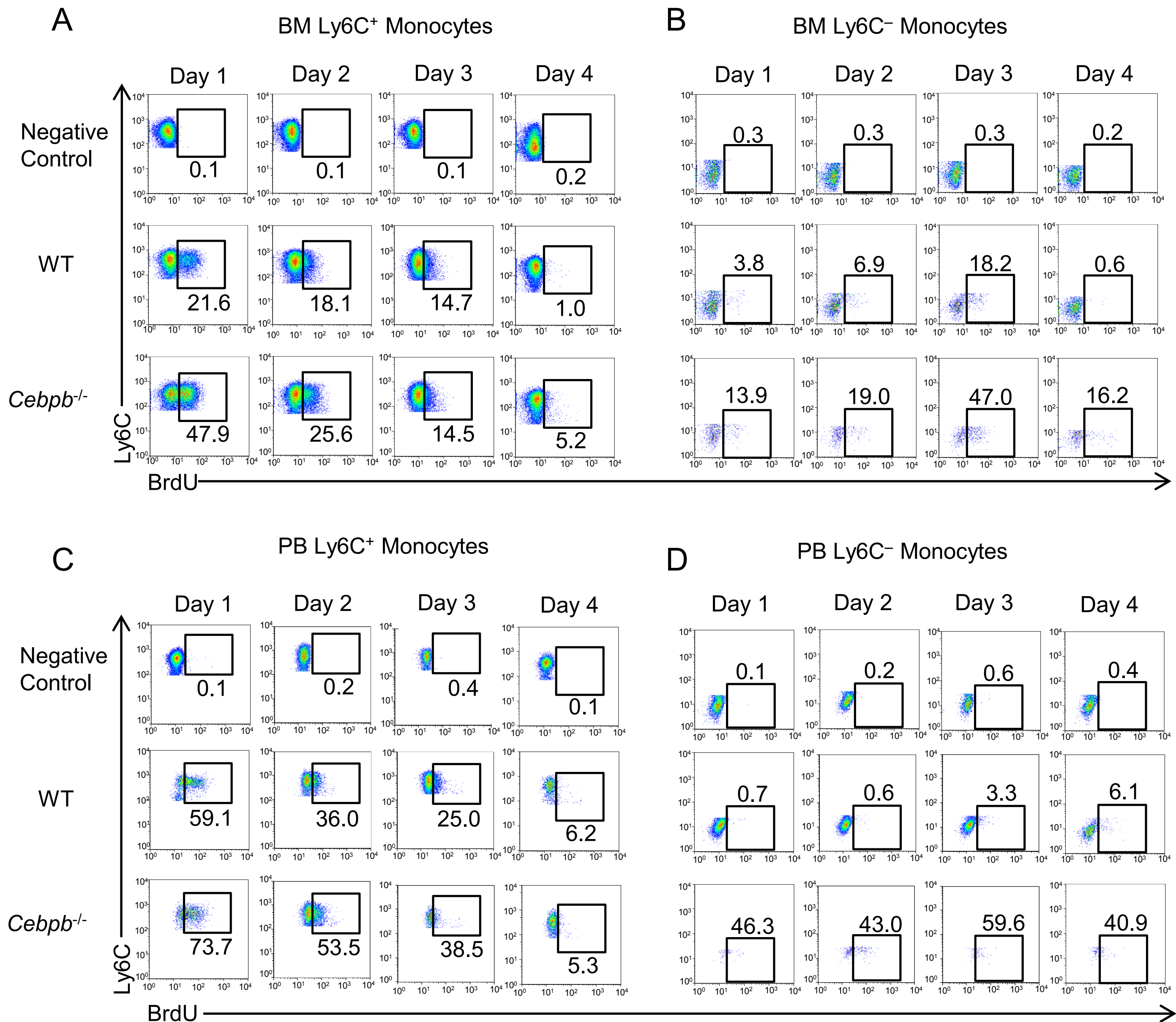

Figure S5

BrdU pulsing experiments reveal accelerated turnover of *Cebpb*–/– monocytes.

Dynamics of monocyte subsets in WT and *Cebpb*–/– mice are shown. (A–D) Flow cytometric analysis of BrdU+ among monocyte subsets from WT or *Cebpb*–/– mice after BrdU pulsing. Numbers indicate the percentage of cells in the adjacent boxed area. Negative controls were WT mice not injected with BrdU.

Supplemental Fig.6

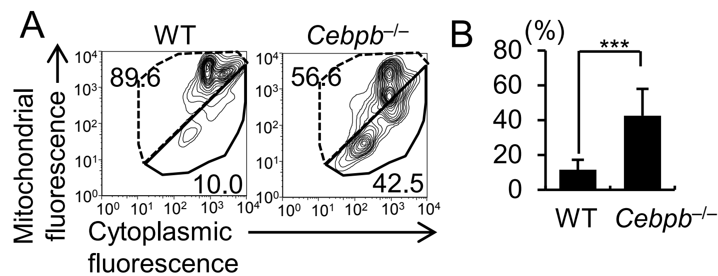

Figure S6
Death of Ly6C⁻ monocytes is accelerated in *Cebpb*$^{-/-}$ mice.
Mouse PB cells were stained using the MitoPTJC-1 Assay Kit (ImmunoChemistry Technologies, MN, USA) according to the manufacturer's protocols after staining for cell surface markers. Mitochondrial red fluorescence and cytoplasmic green fluorescence were analyzed using a FACSCantoII instrument. APC-conjugated anti-CD11b (M1/70), PE-Cy7-conjugated anti-F4/80 (BM8), and V450-conjugated anti-Ly6C antibodies were used. $CD11b^{+}$ $F4/80^{+}$ $FSC^{low\text{-}int}$ SSC^{low} cells were defined as monocytes in this experiment. (A) Mitochondrial membrane potential of $Ly6C^{-}$ monocytes from WT and *Cebpb*$^{-/-}$ mice. Numbers indicate the percentage of cells with normal (dotted lines) and depolarized (filled lines) mitochondria. (B) Frequencies of $Ly6C^{-}$ monocytes with depolarized (apoptotic) mitochondria from WT and *Cebpb*$^{-/-}$ mice (n=6). Data are presented as mean ± SD.

Supplemental Fig.7

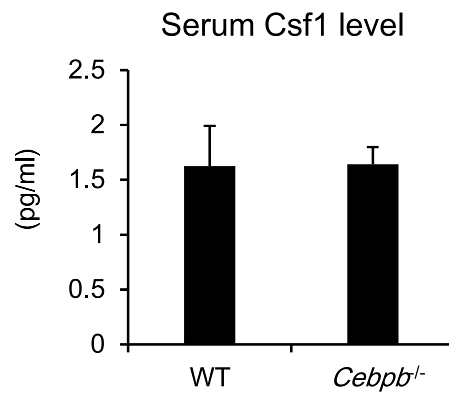

Figure S7
The serum Csf1 level is identical in WT and *Cebpb*$^{-/-}$ mice.
The Csf1 level in serum samples obtained from WT (n=6) and *Cebpb*$^{-/-}$ (n=7) mice was measured using an ELISA. Data are presented as mean $\pm$ SD.

Supplemental Fig.8

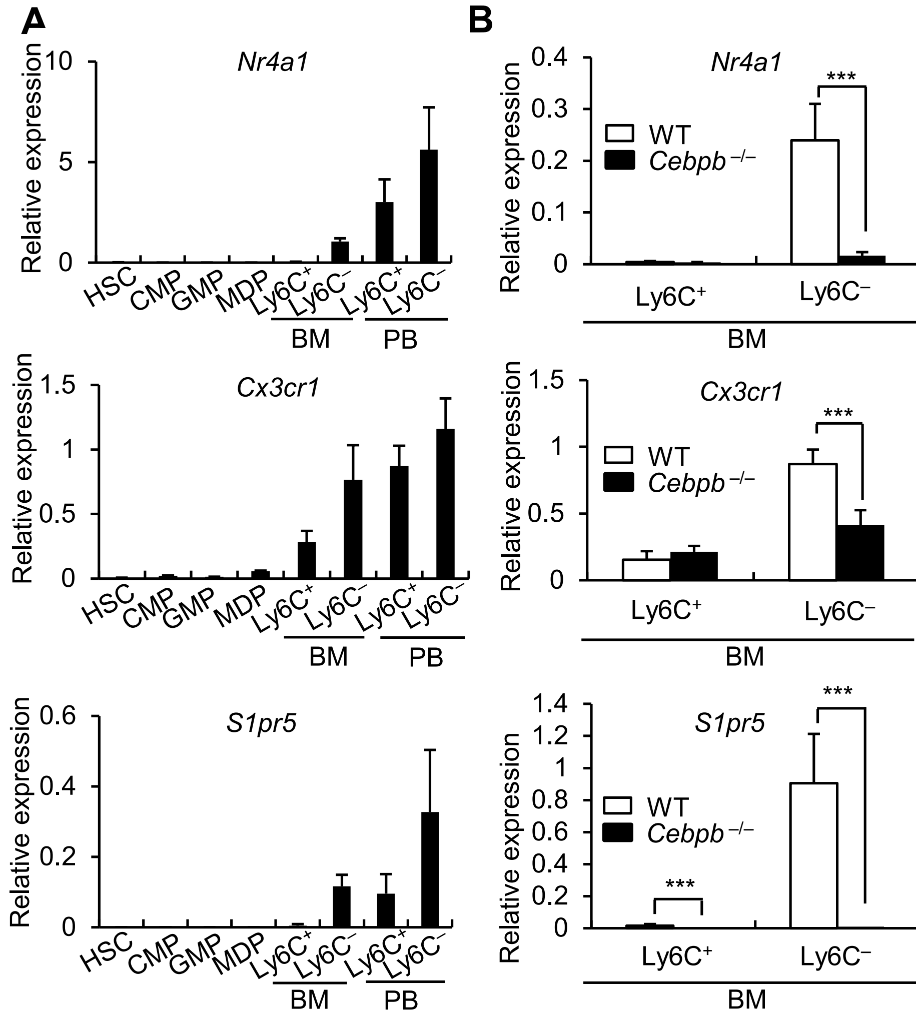

Figure S8

mRNA expression of molecules known to be required for the development of Ly6C⁻ monocytes.

(A and B) mRNA expression of *Nr4a1*, *Cx3cr1*, and *S1pr5* in the indicated cell populations (n=3). Data are presented as the mean ± SD. ***p<0.001.

Supplemental Fig.9

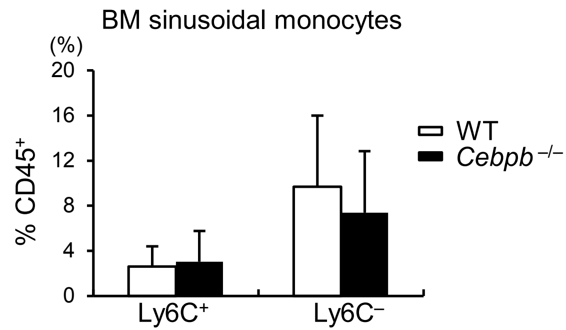

Figure S9

Egress of $Ly6C^{-}$ monocytes from BM is not impaired in *Cebpb*$^{-/-}$ mice.

To label cells in BM sinusoids, mice were intravenously injected with a PE-conjugated anti-CD45 antibody and sacrificed 2 min later. BM was then analyzed by flow cytometry. The percentages of $CD45^{+}$ cells within the indicated monocyte subsets are shown. Data are presented as mean $\pm$ SD.

Supplementary Table 1: Primers used for quantitative real-time PCR

Primer sequences (in 5'-3' direction) and TaqMan probes (Universal Probe Library, Roche Diagnostics) used for quantitative real-time PCR.

Gene name	Forward primer	Reverse primer	Universal probe No.
Cebpb	ATCGACTTCAGCCCCTACCT	TAGTCGTCGGCGAAGAGG	55
Nr4a1	AGCTTGGGTGTTGATGTTCC	AATGCGATTCTGCAGCTCTT	1
S1pr5	GGAGTGCCGGTTACAGGAG	GAAGGACAATAACCTCACTCACC	70
Ccr2	ACCTGTAAATGCCATGCAAGT	TGTCTTCCATTTCCTTTGATTTG	27
Cx3cr1	AAGTTCCCTTCCCATCTGCT	CAAAATTCTCTAGATCCAGTTCAGG	10
Mx1	TTCAAGGATCACTCATACTTCAGC	GGGAGGTGAGCTCCTCAGT	53
Gpadh	TGTCCGTCGTGGATCTGAC	CCTGCTTCACCACCTTCTTG	80